Online ISSN 1848-3380, Print ISSN 0005-1144
ATKAFF 54(3), 364–375(2013)

Danijel Pavković, Nenad Kranjčević, Milan Kostelac

Design of Normal Force Control System for a Pin-on-Disk Tribometer including Active and Passive Suppression of Vertical Vibrations

DOI 10.7305/automatika.54-3.368
UDK 681.532.013:621.8.034(620.19)
IFAC 4.7; 3.2.1

Original scientific paper

This paper presents the design of a computer-controlled pin-on-disk tribometer for friction characterization of various friction sliding pairs. The tribometer setup comprises two high-bandwidth servomotors for the control of the rotating disk and the normal load-related spindle drive, as well as a high-precision tri-axial piezoelectric force sensor for normal and tangential forces measurement. Since the spindle drive system is characterized by notable compliance effects, the normal force cascade control system is designed with the aim of vertical vibrations active damping. In order to compensate for the unevenness of the rotating disk surface and associated high-level perturbations in the specimen normal force, the normal force control system is extended with a feedforward compensator of the disk unevenness disturbance, and a dedicated leaf spring suspension system is designed. The effectiveness of the proposed system of vertical vibrations damping is verified experimentally.

Key words: Vibration suppression, Normal force control, Pin-on-disk tribometer

Projektiranje sustava regulacije vertikalne sile tribometra s uzorkom na disku uključujući aktivno i pasivno prigušenje vertikalnih vibracija. U članku je prikazan dizajn računalom upravljanog tribometra s uzorkom na disku za karakterizaciju različitih kliznih parova. Postav tribometra sadrži dva električna servomotora visokih dinamičkih performansi koji se koriste za regulaciju rotacijskog diska i navojnog vretena za generiranje normalne sile, te tro-osni piezoelektrični senzor za mjerenje normalne i tangencijalne sile. Kako je pogon navojnog vretena karakteriziran značajnom elastičnošću, kaskadni sustav regulacije sile je projektiran s ciljem aktivnog prigušenja vertikalnih vibracija. U svrhu kompenzacije značajnih neravnina površine rotacijskog diska i s njima povezanih velikih amplituda perturbacija normalne sile na uzorak, sustav regulacije normalne sile proširuje se unaprijednim kompenzatorom poremećaja uslijed neravnina površine diska, te za tu svrhu namijenjenim sustavom ovjesa s lisnatim oprugama. Učinkovitost predloženog sustava za prigušenje vertikalnih vibracija provjerena je eksperimentalnim putem.

Ključne riječi: prigušenje vibracija, regulacija vertikalne sile, tribometar s uzorkom na disku

1 INTRODUCTION

In tribological research, pin-on-disk tribometers can be conveniently used for characterization of friction of different sliding pairs such as dry clutch facings [1, 2] and other types of mechanical power transmission elements [3]. The results of friction characterization may then be used to enhance the performance of various transmission systems, either by improving material design or by means of more effective controls. However, the tribometer designs in [1-3], intended for stationary (steady-state) friction and material wear testing, cannot be used to characterize dynamic friction effects, such as those due to varying sliding speed and/or normal force, and the relative position (presliding) dependence (see e.g. [4]). In order to provide the capability for testing of these dynamic friction effects, the pin-on-disk tribometer should be servo-controlled, and the variables relevant to dynamic friction effects should be measured by high-precision/high-bandwidth sensors.

This paper presents the fully computer-controlled pin-on-disk tribometer, equipped with high-bandwidth servomotors for the rotating disk and the normal loading spindle drive, high-precision position/speed sensors, and accurate sensors of normal and tangential forces acting upon the friction material specimen. The normal force control system is designed with the aim of compensating for the emphasized normal loading drive compliance and fric-

tion effects, by means of active damping of vertical vibrations and friction compensation. The effect of uneven disk surface profile, which typically causes notable perturbations of the normal force at mid-high slip speeds [5], is dealt with by introducing the feedforward control action based on the pre-recorded disk surface circumferential profile and, ultimately, by designing a dedicated passive suspension system for the friction material specimen carrier. The effectiveness of the proposed pin-on-disk normal force control system and the innovative suspension system is verified experimentally for a wide range of disk slip speeds.

The paper is organized as follows. An overview of the design of pin-on-disk tribometer system, including the passive vibrations suspension system, is given in Section 2. Section 3 presents the tribometer cascade control system structure, including the normal force cascade control system and disk speed control loop. Vertical axis control system active damping tuning procedure based on the damping optimum criterion is also presented in Section 3, along with the active suspension intervention, and the robustness analysis of the normal force linear control system. The results of experimental verification of the proposed tribometer control system for a wide range of operating regimes are included in Section 4. Concluding remarks are given in Section 5.

2 PIN-ON-DISK TRIBOMETER SETUP

2.1 Pin-on-disk system overview

Figure 1 shows the principal schematic of the pin-on-disk tribometer system, where the normal force on the friction material specimen is generated by the vertical axis spindle servodrive, while the relative motion of the friction (sliding) pair is achieved by the speed-controlled disk servodrive. For that purpose, the tribometer comprises two high-bandwidth permanent-magnet synchronous servomotors with current (torque) controllers embedded within their respective power converters ($f_{BW} \approx 80$ Hz). The disk driving motor (with 9.8 Nm rated torque and 6000 rpm rated speed) is coupled to the rotating disk via a belt drive with transmission ratio $i_{bd} = 3$, and characterized by negligible compliance effects. The disk drive is equipped with a high-precision incremental encoder with 2048 sinusoidal pulses per revolution at the motor side (2 million pulses after hardware interpolation) and an additional incremental encoder (5 million pulses effective resolution) for precise disk position/speed measurements.

The tribometer vertical axis servodrive features another synchronous servomotor (with 0.5 Nm rated torque and 6000 rpm rated speed), which is coupled to the friction material specimen carrier through a spindle gear system with a transmission ratio $i_v = 2\pi$ rad/mm, and a leaf spring

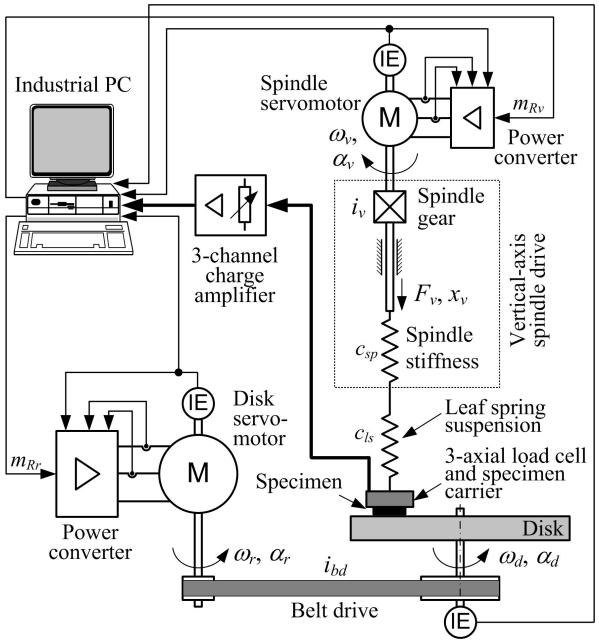

Figure 1. Principal schematic of pin-on-disk tribometer system.

suspension system for the suppression of vertical-axis vibrations caused by the uneven profile of the rotating disk surface (see next subsections). The reaction forces of the specimen carrier are measured by a tri-axial piezoelectric load cell coupled with a corresponding charge amplifier. The force measurement setup can be configured for measurement of specimen normal forces of up to 2000 N, and horizontal forces of up to 600 N. The setup also comprises precise thermocouples for the friction material specimen, force sensor and rotating disk temperature measurements. The overall pin-on-disk tribometer system is controlled by a Pentium 4 industrial PC equipped with appropriate signal acquisition and control cards.

2.2 Disk surface profile

Figure 2 shows the rotating disk surface profile (in vertical direction), recorded within the normal force closed-loop control system (Section 3) for the low speed of the rotating disk ($\omega_d = 1.6$ rpm), whereby the normal force control system could easily follow the vertical axis displacement changes caused by the disk surface unevenness. The recorded results indicate the rotation-dependent disk surface profile shape, with the magnitude of roughly 40 μm peak-to-peak. This rotating-disk disturbance can be compensated either by means of control (see Section 3), or by means of a dedicated passive suspension system (see next subsection).

2.3 Leaf spring suspension system

Figure 3 shows the photograph of the leaf spring suspension system for the suppression of specimen carrier vertical-axis vibrations due to the rotating disk surface unevenness illustrated in Fig. 2. The suspension system comprises three evenly distributed leaf springs, which are designed for a rather low axial stiffness of the normal loading drive (thus being able to absorb the vertical position perturbations without significant force ripple), while simultaneously achieving rather high stiffness for the tangential direction. Moreover, friction between the neighboring spring plates acts as a damper of the disk rotation-induced vibrations. Finally, the leaf spring suspension system is located close to the disc surface in order to inhibit the excitation of specimen carrier vibrations about the transversal axis due to specimen vs. disk friction force (tangential force) variations.

The experimentally recorded vertical-axis stress-strain curves, without and with the leaf spring suspension system, are shown in Fig. 4. The results point out that the vertical-axis servodrive with the suspension system (characterized by the series connection of the leaf-spring and the spindle drive compliance) has a notably lower overall stiffness $c = c_{sp} \cdot c_{ls}/(c_{sp} + c_{ls})$ compared to the case when suspension system is not used ($c = c_{sp}$). Since the normal force perturbations are directly proportional to the disk surface profile changes and the vertical-axis drive stiffness ($\Delta F_v = c\Delta x_v$), the vertical-axis servosystem equipped with the suspension system would be able to provide favorable suppression of the disk rotation-induced normal force disturbances (see results in Section 4).

3 PIN-ON-DISK TRIBOMETER CONTROL SYSTEM

This section presents the pin-on-disk tribometer control system which comprises the disk speed control loop, and the normal force cascade control system extended with nonlinear compensators of friction and disk disturbance effects. The procedures for linear control systems tuning based on the symmetrical optimum and damping optimum criteria are presented and compared. A superimposed control strategy which coordinates the normal force and disk speed control systems during specimen lowering onto the disk is also presented.

3.1 Control system structure

Figure 5 shows the block diagram representation of the normal force control system and disk speed control system. The disk speed control loop is based on a PI speed controller, while the normal force core control strategy comprises a cascade control system, where a superimposed proportional force controller (P controller) commands the reference for the inner proportional-integral (PI) speed controller. The latter approach may be in contrast with the traditional cascade control systems where the position controller typically commands the inner speed control loop [6], and the force control loop is superimposed to the position control loop [7]. However, by avoiding the

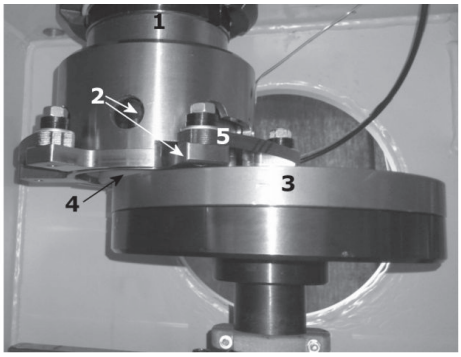

Legend: 1 – leaf spring mount, 2 – sensor head support, 3 – rotating disk, 4 – specimen carrier, 5 – leaf spring.

Figure 3. Photograph of leaf spring suspension system for friction material specimen.

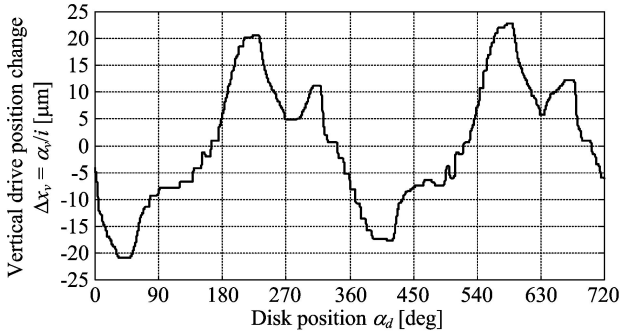

Figure 2. Experimentally recorded disk surface profile (disk speed ω_d = 1.6 rpm).

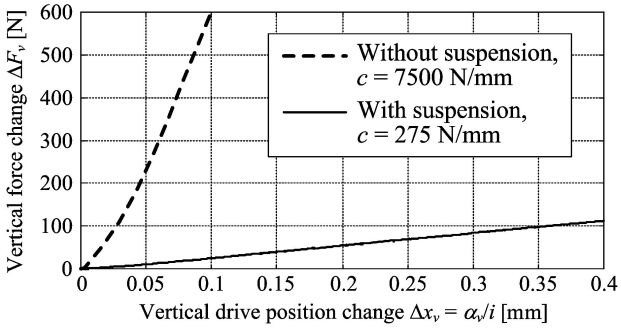

Figure 4. Experimentally recorded vertical axis loading curves.

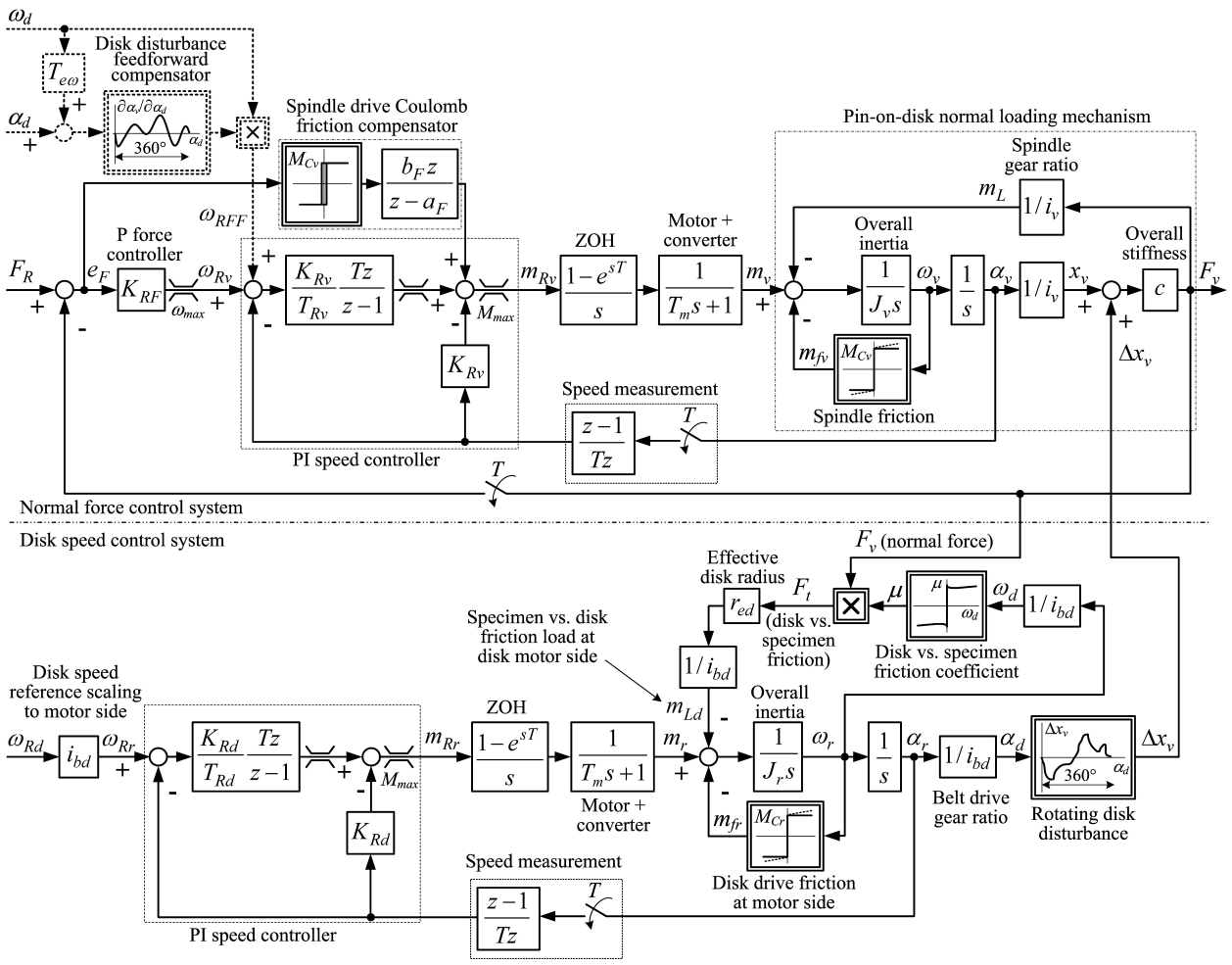

Figure 5. Block diagrams of normal force and disk speed control systems.

inner position control loop altogether, and commanding the speed reference directly through the force controller, a faster force control system response can be obtained.

The normal force cascade control system is extended with a relatively fast nonlinear compensator of Coulomb friction in order to speed up the closed-loop response according to the concept proposed in [8] for the position control system. The compensator comprises a relay term acting upon the force control error e_F, and having the magnitude equal to the estimated Coulomb friction torque. Its output is fed to the innermost torque control loop, where a lag term is added to the compensator output in order to avoid excessive chattering under the steady-state conditions.

The normal force control system can also be extended with a feedforward compensator of the disk unevenness-related disturbance (an active suspension subsystem; dotted blocks in Fig. 5), which is based on the disk disturbance data from Fig. 2. In order to achieve fast disturbance compensation, the compensating signal should be fed to the fast inner speed control loop. Hence, the vertical position vs. disk disturbance look-up data in Fig. 2 needs to be referred to the vertical speed reference as follows:

$$\omega_{RFF} = \frac{d\alpha_v}{dt} = \frac{\partial \alpha_v}{\partial \alpha_d}\frac{\partial \alpha_d}{\partial t} = \frac{\partial \alpha_v}{\partial \alpha_d}\omega_d \qquad (1)$$

For that purpose, the pre-recorded data in Fig. 2 needs to be interpolated in order to obtain a smooth $\alpha_v(\alpha_d)$ estimate, which is then off-line differentiated in order to obtain the vertical position vs. disk position gradient $\partial\alpha_v/\partial\alpha_d$ look-up table. Thus obtained look-up table is supplied by the actual disk position signal projected ahead in time based on the estimated spatial "lag" due to vertical axis speed control loop lag $T_{e\omega}$, and referred to a single disk rotation (i.e. 0 – 360 degree range). The resulting $\partial\alpha_v/\partial\alpha_d$ look-up table output is then modulated with respect to the actual disk speed ω_d according to (1).

3.2 Controller tuning

3.2.1 Normal force control system

The vertical-axis PI speed controller parameters are determined according to the damping optimum criterion [9, 10]. This is a pole-placement-like analytical method of design of a linear continuous-time system with a full or reduced-order controller. The method is based on the closed-loop characteristic polynomial given in the form:

$$A_c(s) = D_2^{n-1} D_3^{n-2} \cdots D_n T_e^n s^n + \cdots + D_2 T_e^2 s^2 + T_e s + 1 \tag{2}$$

where T_e is the closed-loop system equivalent time constant, and $D_2, D_3, \ldots, D_n$ are the characteristic ratios. In the optimal case $D_i = 0.5 (i = 2 \ldots n)$, the closed-loop system of any order n has a quasi-aperiodic step response characterized by an overshoot of approximately 6% and the rise time of approximately 1.8 T_e. By choosing a larger T_e value, the control system robustness is generally improved and the noise sensitivity is decreased, but, in turn, a slower response and less efficient disturbance rejection are obtained. For the case of reduced-order controller, only the dominant characteristic ratios $D_2, D_3, \ldots, D_r (r < n)$ are set to the optimal value of 0.5.

For the purpose of equivalent continuous-time domain design, the combined effect of the sampler and zero-order-hold (ZOH) element and the position differentiation-based speed measurement lag (Fig. 5) may be approximated by the equivalent first-order lag term with the equivalent time constant equal to the controller sampling time T (with T = 2 ms used herein). This "parasitic" lag term can be lumped with the servomotor torque lag term into an equivalent parasitic first-order lag term:

$$G_{par}(s) = \frac{1}{T_\Sigma s + 1}, \tag{3}$$

where $T_\Sigma = T_m + T$ is the lag term equivalent time constant.

Based on the control system block diagram in Fig. 5 and assumption (1), the speed control loop transfer function $G_{c\omega}(s) = \omega_v(s)/\omega_R(s)$ is found to be given by (4):

$$G_{c\omega}(s) = \frac{\dfrac{K_{Rv}}{K_{Rv} + J_v T_{Rv} \Omega_0^2}}{\dfrac{J_v T_{Rv} T_\Sigma s^3}{K_{Rv} + J_v T_{Rv} \Omega_0^2} + \dfrac{J_v T_{Rv} s^2}{K_{Rv} + J_v T_{Rv} \Omega_0^2} + \dfrac{(K_{Rv} + J_v \Omega_0^2 T_\Sigma) T_{Rv} s}{K_{Rv} + J_v T_{Rv} \Omega_0^2} + 1}, \tag{4}$$

where Ω_0 is the natural frequency of vertical vibrations:

$$\Omega_0 = \sqrt{\frac{c}{i_v^2 J_v}}, \tag{5}$$

and J_v is the total inertia of the vertical axis drive referred to the electrical machine shaft.

By equating the coefficients of the closed-loop characteristic polynomial in (4) with the coefficients of the third-order damping optimum polynomial (equation (2) with $n = 3$), and rearranging, the following equations for the PI speed controller parameters are obtained:

$$T_{e\omega} = \frac{T_\Sigma}{D_{2\omega} D_{3\omega}}, \tag{6}$$

$$K_{Rv} = J_v \frac{1 - D_{2\omega} T_{e\omega} T_\Sigma \Omega_0^2}{D_{2\omega} T_{e\omega}}, \tag{7}$$

$$T_{Rv} = T_{e\omega} \frac{1 - D_{2\omega}^2 D_{3\omega} T_{e\omega}^2 \Omega_0^2}{1 - D_{2\omega} T_{e\omega}^2 \Omega_0^2}. \tag{8}$$

Note that, unlike the more commonly used symmetrical optimum tuning method [6] (used for the tuning of the disk drive PI speed controller, see next subsection), the proposed tuning method adjusts the PI speed controller parameters with respect to the natural frequency of vertical vibrations. Thus, it provides favorable damping of drive vibrations by means of control regardless of vertical axis compliance. On the other hand, for the case of unconstrained drive ($c \to 0$), the damping optimum-based PI controller tuning (with characteristic ratios $D_{2\omega}$ and $D_{3\omega}$ set to the optimal value 0.5) becomes equivalent to the symmetrical optimum tuning method (cf. equations (14) and (15) and results in Fig. 6).

For the case of optimal choice of closed-loop characteristic ratios, the speed control loop may be approximated by the equivalent first-order lag term [10]:

$$G_{e\omega}(s) = \frac{K_{e\omega}}{T_{e\omega} s + 1}, \tag{9}$$

with the equivalent gain $K_{e\omega} = K_{c\omega}/(K_{c\omega} + T_{c\omega} J_v \Omega_0^2)$. By taking into account equations (5) and (9), the following normal force control closed-loop transfer function $G_{cF}(s) = F_v(s)/F_R(s)$ is obtained:

$$G_{cF}(s) = \frac{1}{\frac{T_{e\omega}}{i_v J_v \Omega_0^2 K_{e\omega} K_{RF}} s^2 + \frac{1}{i_v J_v \Omega_0^2 K_{e\omega} K_{RF}} s + 1}. \tag{10}$$

Finally, by equating the coefficients of the closed-loop characteristic polynomial in (10) with the coefficients of the second-order damping optimum characteristic polynomial, the force controller parameters are calculated as follows:

$$T_{eF} = \frac{T_{e\omega}}{D_{2F}} = \frac{T_\Sigma}{D_{2F} D_{2\omega} D_{3\omega}}, \tag{11}$$

$$K_{RF} = \frac{1}{K_{e\omega} T_{eF} i_v J_v \Omega_0^2} = \frac{D_{2F} D_{2\omega} D_{3\omega}}{K_{e\omega} T_\Sigma i_v J_v \Omega_0^2}. \tag{12}$$

In order to facilitate the so-called critically-damped closed-loop system response (the fastest response without an overshoot), the force control loop characteristic ratio is set to $D_{2F} = 0.35$. Note that the closed-loop system equivalent time constant T_{eF} only depends on the value of the parasitic time constant T_Σ and the characteristic ratios choice, i.e. the normal force control loop response speed is not dependent on the vertical-axis drive stiffness.

The friction compensator lag term parameters are given by:

$$a_F = e^{-T/T_f},\ b_F = 1 - a_F. \tag{13}$$

where T_f = 20 ms is chosen as a trade-off between the response speed (friction compensation effectiveness) and the noise suppression ability.

3.2.2 Disk speed control system

The disk speed control loop also comprises a discrete-time (digital) proportional-integral (PI) speed controller (Fig. 5). Since the disk drive is characterized by negligible compliance effects (due to rather "stiff" belt drive), the PI speed controller can be tuned according to the symmetrical optimum tuning procedure [6], which gives a fast and well-damped response of the speed control loop (J_r is the equivalent disk drive inertia referred to servomotor shaft):

$$T_{Rd} = 4T_\Sigma, \tag{14}$$

$$K_{Rd} = \frac{J_r}{2T_\Sigma}. \tag{15}$$

3.3 Normal force control system damping and robustness analysis

The normal force closed-loop response damping is analyzed for a wide range of vertical axis stiffness c (natural frequency Ω_0) values, based on the root locus plots of the full-order normal force control loop transfer function, obtained by combining the speed control loop transfer function (4) and equation (5):

$$G_{cF}(s) = \frac{F_v(s)}{F_R(s)} = \frac{K_{RF} i_v J_v \Omega_0^2 G_{c\omega}(s)}{s + K_{RF} i_v J_v \Omega_0^2 G_{c\omega}(s)}. \tag{16}$$

In order to illustrate the effectiveness of the active damping tuning procedure based on damping optimum criterion, it is compared to the case when the vertical-axis drive speed control loop is tuned according to symmetrical optimum criterion (see equations (14) and (15)). The normalized root-locus plots in Fig. 6 indicate that the normal force control loop with P force controller and PI speed controller tuned for active damping is indeed characterized by well-damped conjugate-complex pole locations, which do not depend on vertical axis stiffness c (natural frequency Ω_0) values. In the case when the PI speed controller is tuned according to symmetrical optimum, favorable well-damped locations of the conjugate-complex pole pair are obtained only in the case of very "soft" vertical axis compliance (low Ω_0).

The robustness of the normal force control system to

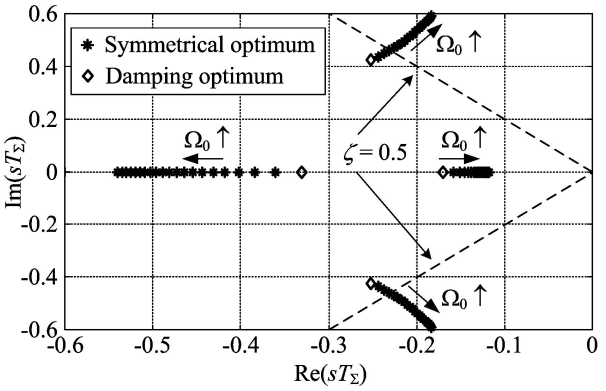

Figure 6. Comparative root-locus plots of normal force cascade control system with speed control loop tuned according to damping optimum and symmetrical optimum.

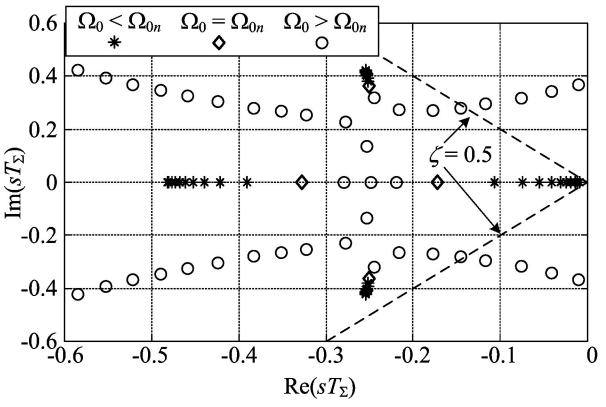

Figure 7. Root-locus plots of normal force cascade control system tuned for active damping in presence of natural frequency parameter variations.

natural frequency Ω_0 (stiffness coefficient c) variations is

also analyzed by means of root-locus method. Figure 7 shows the results of the robustness analysis for the case of damping optimum-based controller tuning in the presence of natural frequency Ω_0 variations with respect to its nominal (actual) value Ω_{0n}. These results point out that the normal force cascade control system tuning with the natural frequency parameter Ω_0 lower than its nominal value ($\Omega_0 < \Omega_{0n}$) results in shifting of the dominant real closed-loop pole towards the s-plane origin (i.e. slower closed-loop response), while at the same time the less-dominant conjugate-complex pole pair remains well-damped. If, on the other hand, the cascade control system is tuned with the natural frequency parameter larger than the nominal one ($\Omega_0 > \Omega_{0n}$), the closed-loop conjugate-complex pole pair is shifted towards poorly-damped (or even unstable) locations.

3.4 Specimen touchdown strategy and coordination with disk speed control system

In order to facilitate a relatively fast specimen lowering onto the disk (touchdown) and coordinate the operation of vertical axis and disk servodrives, the normal force and disk speed control systems in Fig. 5 are extended with a superimposed control strategy. The strategy comprises the specimen touchdown detection logic and a related vertical drive stopping intervention aimed at preventing the vertical force excess after the specimen touchdown.

The simplified block diagram representation of the superimposed control strategy is shown in Fig. 8. The friction material specimen lowering is initiated by the START flag (pulse) which resets the flip-flops. Thus, the vertical servodrive is switched into the speed control mode (i.e. the specimen normal force feedback is disconnected), and a zero speed reference ($\omega_{Rd} = 0$) is commanded to the disk servodrive in order to keep it at standstill. The friction material specimen is then quickly lowered onto the disk from the initial position by commanding a relatively large speed reference value ω_{Rvl} to the vertical axis servodrive, thus facilitating a relatively fast establishing of specimen vs. disk contact (touchdown). The touchdown is detected by means of a simple threshold logic (lower portion of Fig. 8), which switches the control to the normal force controller after the delay interval of $2T_{e\omega}$ (corresponding to vertical speed control loop response time). During the aforementioned delay interval the vertical speed reference ω_{Rv} is briefly reversed (i.e. $\omega_{Rv} = -\omega_{Rvl}$) in order to reduce the vertical position excess after touchdown, which might otherwise lead to a notable normal force overshoot after the high-speed specimen-disk collision (impact). Finally, after the normal force settles close to the desired force value (reference F_R), the disk speed reference ω_{Rd} is applied (after a short delay to ensure robust detection), thus starting the disk servodrive.

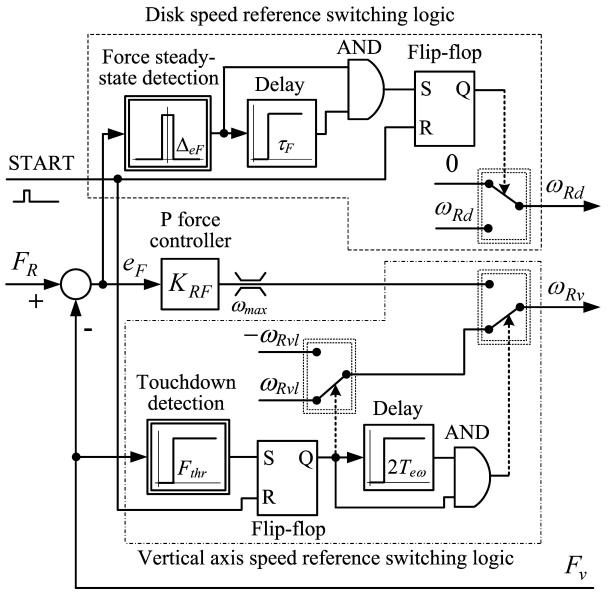

Figure 8. Simplified block diagram of superimposed strategy.

4 EXPERIMENTAL RESULTS

Results of experimental identification of vertical axis and disk drive inertia parameters are shown in this section. The proposed pin-on-disk tribometer control system has been implemented and experimentally validated for a wide range of operating regimes. The effectiveness of the proposed normal force control system is also illustrated for the case of friction coefficient recording for an automotive dry clutch facing material on the steel surface.

4.1 Drive parameters identification

In order to tune the disk drive and vertical axis drive control strategies, the main drive parameters (i.e. the drive equivalent inertias J_r and J_v, the servomotor torque response time constant T_m, and the Coulomb friction torque M_{Cv} in the case vertical axis drive) are estimated by means of the so-called drive starting and stopping experiment (see e.g. [11]). The parameter estimation procedure is based on the drive motion equations for the drive starting ($_I$) under constant torque M_m (facilitated by applying stepwise torque reference change to the torque/current control loop) and overall inertia J stopping under zero motor torque due to friction torque M_f ($_I I$):

$$M_m - M_f = J\frac{d\omega_I}{dt}, \tag{17}$$

$$M_f = -J\frac{d\omega_{II}}{dt}. \tag{18}$$

The results of disk drive and vertical drive starting and stopping experiments are shown in Fig. 9. The starting

and stopping curves in the upper plots are interpolated by fourth-order polynomials over an arbitrary speed range [ω_l, ω_u] (see Fig. 9a), in order to calculate the "noise-free" time-derivatives of the speed curves. The resulting inertia and speed-dependent friction torque estimates, as well as the estimated Coulomb friction torque values for both drives are shown in Fig. 9b.

Figure 10 shows the details of the speed responses of vertical axis drive and disk drive immediately after the torque reference step change, including the linear trend-lines (dash-dot lines). The responses indicate that the equivalent initial speed delays for both drives are around 3 ms. Since the equivalent delay of speed measurement (based on time-differentiation of the measured position) equals half the sampling time ($T/2$ = 1 ms) [12], the torque response delays T_m for both drives are equal to approximately 2 ms.

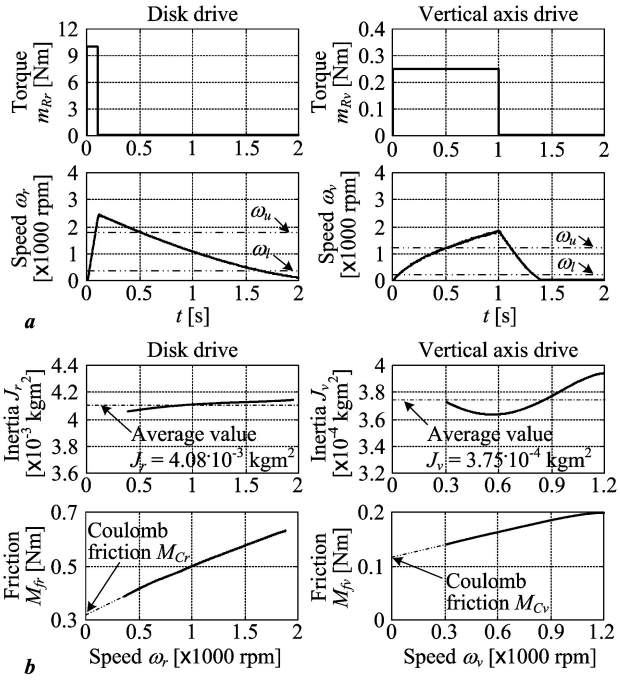

Figure 9. Comparative results of starting and stopping experiments (a), and estimated drive inertia and friction (b) for disk drive and vertical axis drive.

4.2 Control system verification

Figure 11 shows the reference step responses of the vertical axis normal force control system and the disk drive speed control sytem. The comparative normal force step responses without and with a suspension system for the case of rotating disk at standstill ($\omega_d = 0$) are shown in Fig. 11a. These results clearly show that the proposed

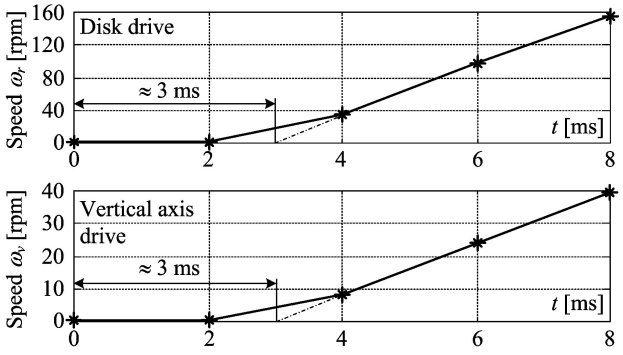

Figure 10. Initial details of motor speed responses during drive starting.

control system ensures favorable damping of the normal force response, while achieving the same response speed (75 ms response time), regardless of the vertical axis stiffness c. Note, however, that in the case of the compliant suspension (smaller c), the speed and torque control efforts become more emphasized. The disk speed control loop responses under zero load conditions ($F_v = 0$), shown in Fig. 11b, indicate that the disk drive speed control system is also characterized by a well-damped response, which is also rather fast (30 ms response time is obtained) because the disk speed control system does not comprise an outer control loop.

Figure 12 shows the comparative responses of the superimposed control strategy (Fig. 8) during relatively high-speed specimen lowering onto the disk ($\omega_{Rv} = 330$ rpm) without and with brief reversal of speed reference after touchdown for the case of leaf spring suspension. In the case of drive stopping under zero speed reference after touchdown detection (speed reference reversal not applied), a notable position excess occurs, which, in turn, results in a notable vertical force overshoot. Note that this force overshoot would be even higher for the case of vertical axis drive without leaf spring suspension (characterized by much higher vertical-axis stiffness c). On the other hand, by briefly reversing the vertical-axis speed reference after the touchdown, the drive can be stopped more quickly (resulting in a much smaller position excess), and the force response overshoot due to specimen vs. disk collision (impact) can be effectively avoided. As a result of brief speed reversal, a somewhat faster normal force settling can be achieved, which ultimately leads to faster starting up of the disk servodrive after the force settling is safely detected (see the final portion of disk speed responses in Fig. 12).

The effectiveness of the overall normal force control system (including vertical axis friction compensation and disk unevenness-related disturbance compensation) is ex-

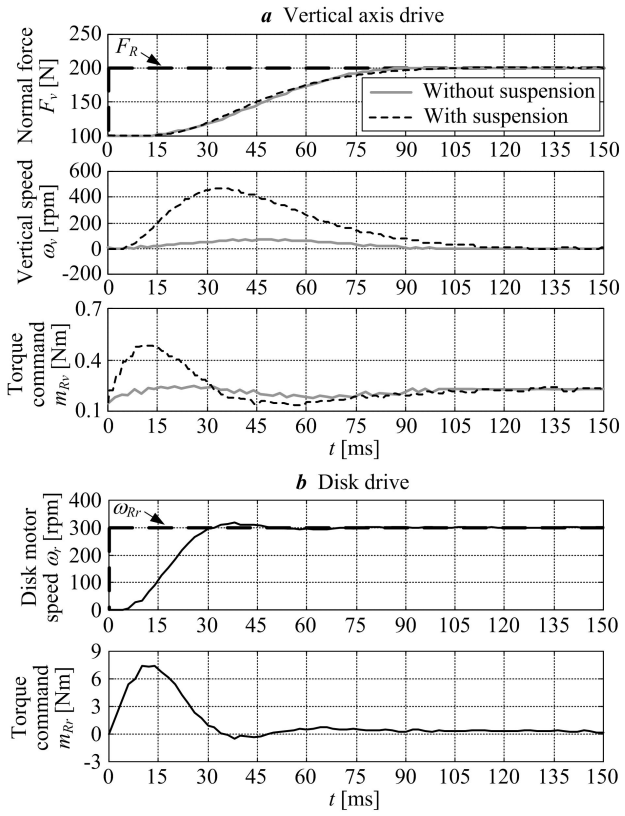

Figure 11. Comparative force reference step responses of normal loading servosystem without and with suspension system for disk at standstill (a), and disk drive speed control system response under zero load (b).

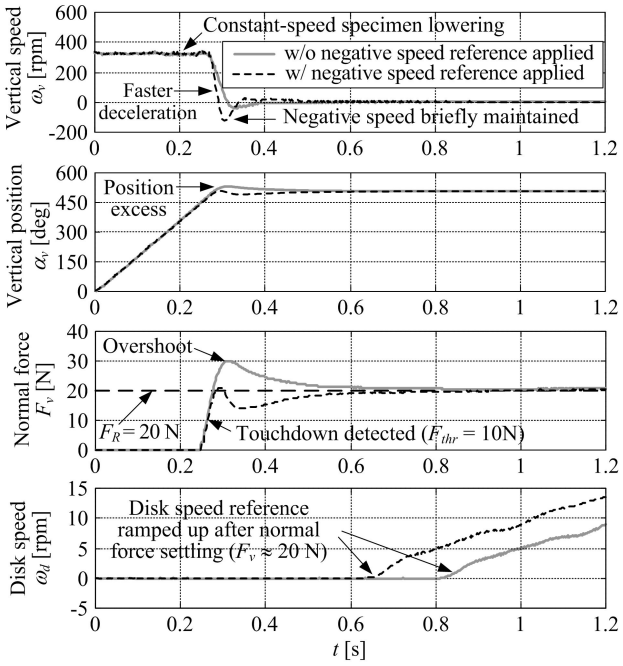

Figure 12. Comparative responses of superimposed control strategy for specimen lowering/touchdown without and with brief application of negative vertical speed reference (with leaf spring suspension).

amined first for the vertical axis drive without the suspension system and under constant disk speed conditions. The results in Fig. 13a, for the disk speed reference $\omega_{Rd} = 33$ rpm, show that the normal force control system without disk disturbance compensation is subject to significant perturbations of normal force. By applying the disturbance compensator, these perturbations are actively suppressed, i.e. the RMS value of normal force perturbations is reduced three-fold. In this case, the rather "stiff" disk speed controller is able to effectively suppress the relatively slow load torque disturbance due to normal force variations, thus keeping the disk speed close to the target value. However, for a ten-fold higher disk speed reference ($\omega_{Rd} = 330$ rpm), the disk disturbance compensator is much less effective due to the bandwidth limitations of the vertical drive speed control loop and the friction compensator, and magnitude of force perturbations approximately reaches $\pm$200N for the 200N normal force reference (Fig. 13b). The effect of extreme normal force perturbations also becomes visible in the disk speed responses (around 10 rpm disk speed variations can be now observed), because the disk speed controller cannot fully suppress the related "fast" variations of the normal force-related disturbance torque at disk servomotor side.

Figure 14a shows that the introduction of the leaf-spring suspension system results in a substantial suppression of normal force variations due to disk disturbance at both low and high disk speeds, even without the disk disturbance compensation. Namely, the RMS values of normal force perturbations are reduced up to two orders of magnitude compared to the results in Fig. 13b, thus making the disk disturbance compensator redundant in the case when the suspension system is applied. As expected, the application of leaf spring suspension, and related attenuation of normal force perturbations, also benefits the disk speed control system, which is now characterized by low magnitudes of disk speed variations (less than 1 rpm) even at high disk speeds (Fig. 14b).

4.3 Friction coefficient recording

The effectiveness of the proposed normal loading servosystem with suspension-based suppression of disk disturbances is further illustrated in Fig. 15 for the case of harmonic disk speed shape, which is convenient for the recording of the friction coefficient vs. slip speed curve

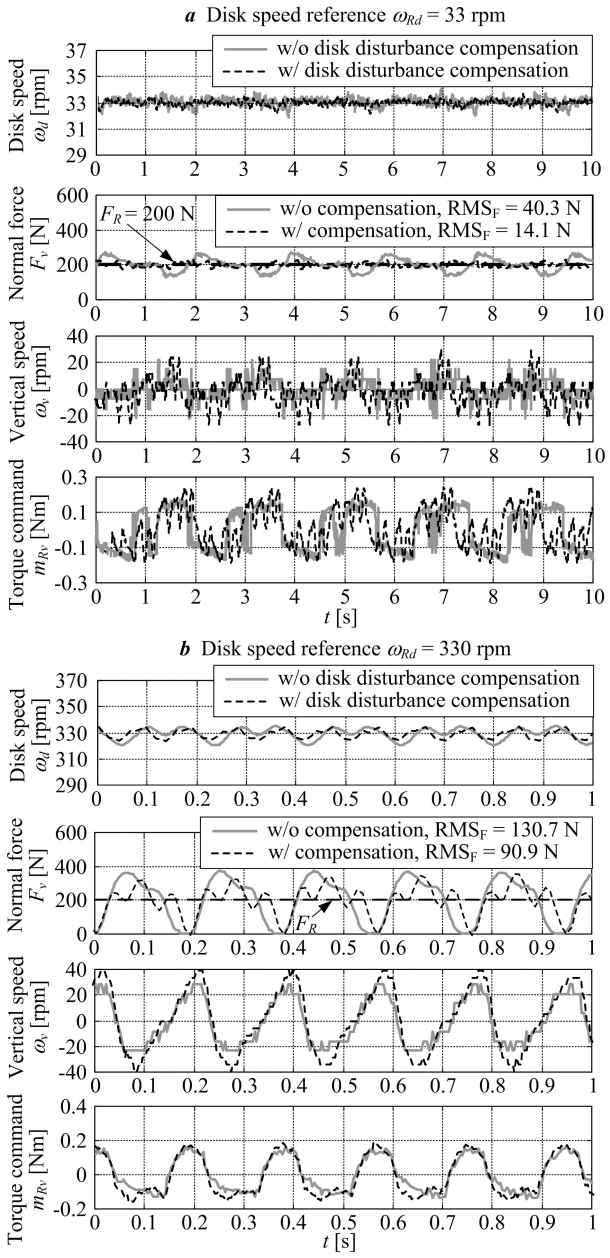

Figure 13. Comparative results of normal force control without and with disk disturbance feedforward compensation (friction compensator is active, no passive suspension).

[4]. In order to remove the noise from the reconstructed friction coefficient $\mu = F_t/F_v$ (middle plot in Fig. 15a), the friction coefficient is filtered by a two-sided (forward-backward) fourth-order Butterworth low-pass filter with a cutoff frequency of 3 Hz. The friction coefficient is then averaged over each period of the harmonic speed shape, thus resulting in a smooth (hysteresis-free) estimate of the

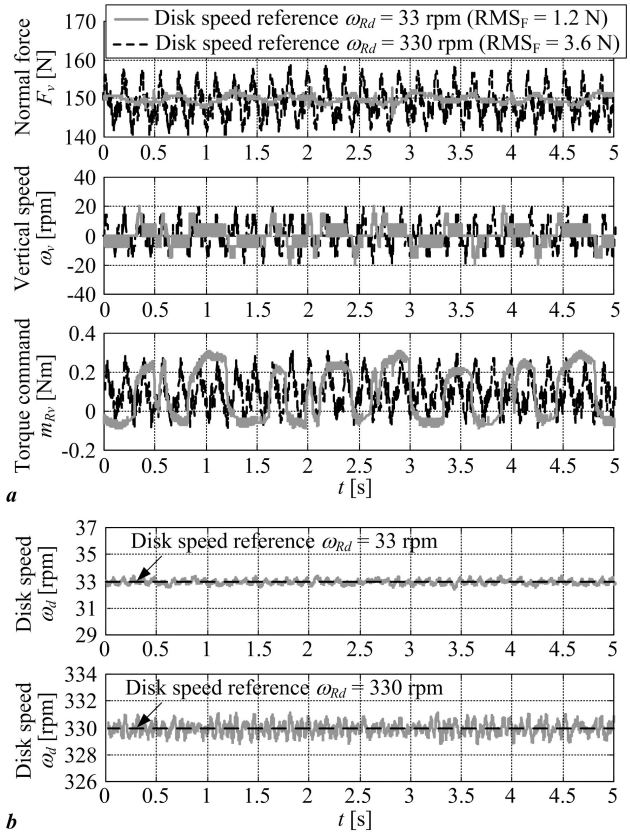

Figure 14. Comparative normal force control results with suspension system included for different disk speed references (a), and related disk speed responses (b) with disk disturbance compensator turned off.

friction coefficient vs. slip speed static curve, as shown in Fig. 15b.

5 CONCLUSION

The paper has outlined a fully servo-controlled pin-on-disk tribometer design, equipped with high-bandwidth servomotors, a precise tri-axial load cell for the measurement of normal and tangential forces acting upon the friction material specimen, and a dedicated suspension system. For the purpose of precise control of normal force acting upon the friction material specimen, a cascade force control system has been designed for the vertical-axis spindle drive, comprising an inner proportional-integral (PI) speed controller tuned for active damping of vertical axis vibrations, and the superimposed proportional (P) force controller. The parameters of linear controllers have been determined analytically by using the damping optimum criterion. In order to speed up the normal force response and to suppress the rotating disk unevenness disturbance effect, a nonlinear compensator of spindle drive friction and a disk

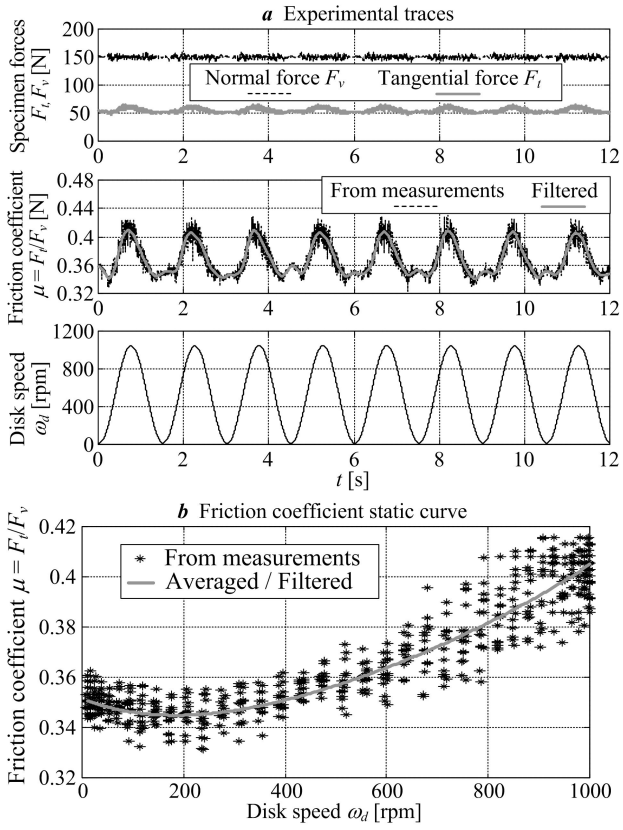

Figure 15. Results of experimental recording of friction coefficient data.

disturbance feedforward compensator have been included in the overall normal force control strategy. A superimposed control strategy comprising coordination between the normal force control system and the disk speed control system during specimen lowering onto the disk has also been designed.

The effectiveness of the proposed overall control strategy has been verified experimentally. The results have shown that the proposed normal force control strategy without the dedicated suspension system can only be effective against the rotating disk disturbance at relatively low disk speeds, mainly due to a limited bandwidth of the vertical axis speed control loop and the spindle drive friction compensator. The aforementioned normal force control strategy limitations may also result in notable disk speed perturbations at higher disk speeds where the disk speed controller, even though tuned for fast response, cannot fully suppress the related normal force disturbance at motor side. By fitting the normal loading servosystem with the dedicated passive suspension system, the overall control strategy has been able to suppress the disk-induced disturbance effects over a wide speed range. Ultimately, this has facilitated the effective utilization of the tribometer for the accurate reconstruction of the friction coefficient vs. slip speed static curve (Stribeck curve).

Future work is going to be directed towards detailed characterization of different friction pairs, with the emphasis on different dynamic friction effects, including varying normal force conditions.

ACKNOWLEDGMENT

This work was supported by the Ministry of Science, Education and Sports of the Republic of Croatia through the R&D project "Computer-Controlled Friction Testing Machine", grant No. 5068.

References

[1] M. Bezzazi, A. Khamlichi, A. Jabbouri, P. Reis, J. P. Davim, "Experimental Characterization of Frictional Behaviour of Clutch Facings using Pin-on-Disk Machine", *Materials and Design*, Vol. 28, No. 7, pp. 2148–2153, 2007.

[2] A. Khamlichi, M. Bezzazi, A. Jabbouri, P. Reis J. P. Davim, "Optimizing Friction Behavior of Clutch Facings using Pin-on-Disk Test", *International Journal of Physical Sciences*, Vol. 3, No. 2, pp. 65-70, 2008.

[3] S. K. Sinha, S.-L. Thia, L. C. Lim, "A New Tribometer for Friction Drives", *Wear*, Vol. 262, No. 1–2, pp. 55–63, 2007.

[4] B. Armstrong-Hélouvry, P. Dupont, C. Canudas de Wit, C, "A Survey of Models, Analysis Tools and Compensation Methods for the Control of Machines with Friction", *Automatica*, Vol. 30, No. 7, pp. 1083-1138, 1994.

[5] I. Garcia-Prieto, M. D. Faulkner, J. R. Alcock, "The Influence of Specimen Misalignment on Wear in Conforming Pin on Disk Tests", *Wear*, Vol. 257, No. 1-2, pp. 157–166, 2004.

[6] W. Leonhard, *Control of Electrical Drives*, 3rd ed., Berlin, Germany: Springer-Verlag, 2001.

[7] J. J. Gorman, N. G. Dagalakis, "Force Control of Linear Motor Stages for Microassembly", in *Proceedings of 2003 ASME International Mechanical Engineering Congress and Exposition - IMECE 2003* (Washington, D.C., USA), November 2003.

[8] J. Deur, D. Pavković, N. Perić, M. Jansz, D. Hrovat, "An Electronic Throttle Control Strategy Including Compensation of Friction and Limp-Home Effects", *IEEE Transactions on Industry Applications*, Vol. 40, No. 3, pp. 821–834, 2004.

[9] P. Naslin, *Essentials of Optimal Control*, London, UK: Iliffe Books Ltd, 1968.

[10] J. Deur, *Design of linear servosystems using practical optima*, Internal memorandum 04/19/2001 (translation of Chap. 3 of Ph. D. Thesis by J. Deur), Faculty of Mechanical Engineering and Naval Architecture, University of Zagreb, Croatia, 2001.

[11] J. Deur, M. Kostelac, Z. Herold, V. Ivanović, D. Pavković, M. Hrgetić, J. Asgari, C. Miano, D. Hrovat, "An In-Wheel Motor-Based Tyre Test Vehicle", *International Journal of Vehicle System Modelling and Testing*, Vol. 2, No. 3, pp. 252–275, 2007.

[12] K. Saito, K. Kamiyama, T. Ohmae, T. Matsuda, "A Microprocessor-Controlled Speed Regulator with Instantaneous Speed Estimation for Motor Drives", *IEEE Transactions on Industrial Electronics*, Vol. 35, No. 1, 1988.

Danijel Pavković received his B.Sc. and M.Sc. degrees in Electrical Engineering in 1998 and 2003, respectively, and his Ph.D. degree in Mechanical Engineering in 2007, all from the University of Zagreb, Croatia. He is currently holding the position of an Assistant Professor at the Faculty of Mechanical Engineering and Naval Architecture, University of Zagreb, teaching subjects in the field of electrical machines, electrical servodrive control, and digital control systems. He has participated on 14 research and technology projects supported by the Ministry of Science of the Republic of Croatia, Croatian Science Foundation, Ford Motor Company, Jaguar Cars Ltd., and the CROSCO Integrated Drilling & Well Services Company. His research interests include estimation and control of electrical servodrive systems with automotive applications, and energy storage systems modeling, estimation and control.

Nenad Kranjčević is an Associate Professor at the Department of Design, Faculty of Mechanical Engineering and Naval Architecture, University of Zagreb. He obtained his B.Sc., M.Sc. and Ph.D. degrees in Mechanical Engineering in 1990, 1994 and 2000 respectively, all from the University of Zagreb, Croatia. His teaching subjects are in the field of machine elements and design with respect to manufacturing processes. His research interests are in dynamics and vibrations of mechanical systems, which is founded on his previous work and employment at the Department of Engineering Mechanics at the same Faculty. He has participated in 5 research projects supported by the Ministry of Science of the Republic of Croatia and a collaboration project supported by the European Commission within the Framework Programme FP7.

Milan Kostelac is employed by the Mechanical Handling Equipment and Constructions Chair at the Faculty of Mechanical Engineering and Naval Architecture University of Zagreb (UNIZAG FSB) as an Assistant Professor. Doctoral thesis "Influence of Direct Drive on structure of Drive Mechanisms" is defended in 2006 at the Faculty of Mechanical Engineering and Naval Architecture, University of Zagreb. He participated in the Implementation of several projects in Croatia, and he worked as member of the team on several international projects related to the development of Mechatronic Mobile Systems. He has published several scientific papers in his immediate field of expertise and has successful collaboration with the industry in the development of Projects, Studies, Reports and Technical Expertises.

AUTHORS' ADDRESSES

Asst. Prof. Danijel Pavković, Ph.D.
Prof. Nenad Kranjčević, Ph.D.
Asst. Prof. Milan Kostelac, Ph.D.
Faculty of Mechanical Engineering and Naval Architecture,
University of Zagreb,
Ulica Ivana Lučića 1, HR-10000, Zagreb, Croatia
email: {danijel.pavkovic, nenad.kranjcevic,
milan.kostelac}@fsb.hr

Received: 2012-09-22
Accepted: 2013-01-10